COBEM 2023 27TH INTERNATIONAL CONGRESS OF MECHANICAL ENGENEERING

ABCM Brazilian Society of Mechanical Sciences and Engineering
27th ABCM International Congress of Mechanical Engineering
December 04-08, 2023, Florianópolis-SC, Brazil

# COB-2023-1439
# INVESTIGATION OF THE DYNAMIC BEHAVIOR OF REINFORCED BEAMS

**Lucas Henrique Bastos Oliveira**
**Vinícius Germanos Cleante**
**Thiago de Paula Sales**
**Domingos Alves Rade**
Aeronautics Institute of Technology - Mechanical Engineering Division - 50 Mal. Eduardo Gomes Sq., Vila das Acácias, Zip code: 12.228-900, São José dos Campos, São Paulo, Brazil.
lucaslhbo@ita.br, cleante@ita.br, tpsales@ita.br, rade@ita.br

***Abstract.*** *Reinforced beams have applications in various engineering fields, such as civil, aeronautical, naval, and maintenance engineering. Models based on the finite element method (FEM) are widely used to investigate the dynamic behavior of these structures. However, accurately describing high-frequency phenomena with FEM can demand significant computational effort due to the need for refined meshes. The Spectral Finite Element Method (SFEM) emerges as an alternative to address this issue, allowing the construction of models with few elements that remain highly accurate in high-frequency scenarios. This ongoing work investigates the influence of reinforced layers on the dynamic behavior of a beam with a weakness point at the center. The main objective is to evaluate the influence of the length of the gap and the lengths of the reinforcement layers on the structure's dynamics, with the aim of assessing the potential of reinforcement layers in enhancing structural integrity and exploring new engineering applications. Using the multi-layer beam theory with the Zig-Zag warping theory, the SFEM is derived and validated with results from the FEMAP software. An SFEM model for reinforced beams with different lengths of reinforced layers and various gap lengths is derived and investigated. The results show that increasing the gap length has a detrimental effect of softening the structure. On the other hand, the use of reinforcement layers improves the structural properties. However, it is found that the length of the reinforcement layers in effective contact with the beam is more relevant to improving the dynamic properties of the structure than the total length of the reinforcement layers.*

***Keywords:*** *multi-layer beam, spectral finite element, vibration, numerical simulation.*

## 1. INTRODUCTION

Reinforced beams find a wide range of applications in civil, aerospace, naval, and mechanical engineering (Hart-Smith, 1973a; Hart-Smith, 1973b; Hollaway and Cadei, 2002; Zhao and Zhang, 2007; Perrut, 2018). The use of reinforcement layers enhances the stiffness of these structures, making them suitable for applications in civil engineering, such as concrete reinforced beams, as well as for joining multiple structures in aeronautical and naval maintenance and connecting energy conductor cables with splices. Understanding and modeling the dynamic behavior of such reinforced structures is essential to ensure their safety and improve their performance and the use of multi-layer models is an effective approach to investigate reinforced beams, because it avoids the need to use contact formulation, reducing the models' complexity.

Different methods have been used to predict structure dynamics, such as Finite Element Method (FEM), Dynamic Stiffness Method (DSM) and Spectral Finite Element Method (SFEM) (Lee, 2009; Doyle, 2012). For instance, Banerjee and Sobey (2005) proposed a model for a three-layered sandwich beam based on the DSM. In their model, they assumed the upper and the bottom layers as Rayleigh beams and the middle layer as Timoshenko beam, each with different material properties. Later, assuming all layers were modeled as a Timoshenko beam with different thicknesses, Banerjee *et al.* (2007) investigated the free vibration characteristic of the structure.

Xu and Wu (2007) developed a plane stress model based on the State Space Method for a two-dimensional composite beam with inter-layer slips using the state space method. To account for the effect of the shear deformation, an equivalent elastic moduli was proposed. Smyczynski and Magnucka-Blandzi (2015) derived a model to predict the structure dynamics of a five-layered sandwich beam consisting of two metal layers, two biding layers and one metal foam core. Su and Banerjee (2015) developed a model based on DSM to investigate the free vibration behavior of functionally-graded Timoshenko beams.

Unal *et al.* (2016) derived a multi-layered beam model using the SFEM including the Zig-Zag theory to account for each individual layer rotation , demonstrating its applicability in structural health monitoring and damage prediction. The authors also derive a model considering a discontinuity on the top layer of the structure. The theoretical results were compared with results obtained from FEM, showing that SFEM allows for the prediction of the structure dynamic using

a smaller number of elements and with much higher accuracy. Sun *et al.* (2018) developed a numerical procedure using a spectral approach to study the dynamic behavior of reinforced concrete beams exposed to fire. Azandariani *et al.* (2022) developed a SFEM model to assess the free vibration characteristics of axially-loaded functionally-graded beam, using the first-order shear deformation theory.

In this context, this ongoing work investigates the use of reinforced layers to bond a beam layer with a weak point at its center. The weakness is introduced by creating a gap, splitting the beam layer in two. Thus, this paper aims to investigate the influence of the length of the gap and the length of the reinforcement layers, to assess the potential use of reinforcement layers to enhance structural integrity. Assuming each layer is modeled as an extended Timoshenko beam, the SFEM multi-layer model with the Zig-Zag theory proposed by Unal *et al.* (2016) is used to derive the dynamic stiffness matrix of the structure. The paper is organized as follows: after the introduction, the modeling methodology is described followed by a numerical validation using FEM software. Later, the influence of the gap and the length of the reinforced layers on the system dynamics are discussed closing with some conclusions.

## 2. PROBLEM STATEMENT AND MODELING

In this section, the model to describe the dynamic behavior of the reinforced beam is presented. Consider the structure shown in Figure 1. It consists of a primary beam layer split into two beams, which form the gap between them, and two reinforcement layers connecting the primary beam. Each layer is assumed to be a uniform beam of rectangular cross-sectional area. The structure can be divided into five subsections, denoted as $A_1$, $A_2$, $B_1$, $B_2$ and $C_1$. The central section, comprising subsections $B_1$, $B_2$ and $C_1$, represents a weakened portion reinforced by two externally bonded layers. In this situation, the left-hand and right-hand parts of the primary beam, separated by a gap, are connected by the external layers. Subsections $A_1$ and $A_2$ consist of single-layer beams of lengths $L_{A_1}$ and $L_{A_2}$, respectively, with only the primary beam. Subsections $B_1$ and $B_2$ consist of three-layers beams of lengths $L_{B_1}$ and $L_{B_2}$, respectively, representing the top and bottom layers as reinforcement for the primary beam placed between them. Subsection $C_1$ consists only of the two reinforcement layers, with a gap of the same length between them, representing the discontinuity between the left and right primary beams.

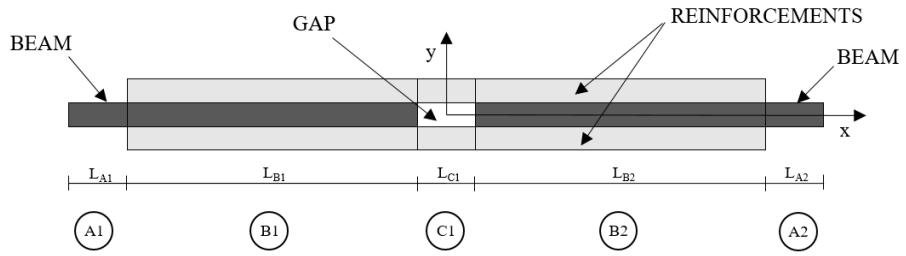


Figure 1. Reinforced beam with gap.

To model the multi-layer beam as depicted in Figure 1, consider first a simple case of the three-layers beam as shown in Figure 2. The formulation will be derived following the work of Unal *et al.* (2016), who presented a formulation based on the Zig-Zag theory, adaptable to an arbitrary number of layers. Each layer is idealized according to the extended Timoshenko beam theory, which adds to the Euler-Bernoulli beam theory the effects of transverse shear and rotatory inertia of the cross-sections and the longitudinal displacement. Here, the developments are adapted for the case of three-layer beams. To simplify the model, the following assumptions are considered:

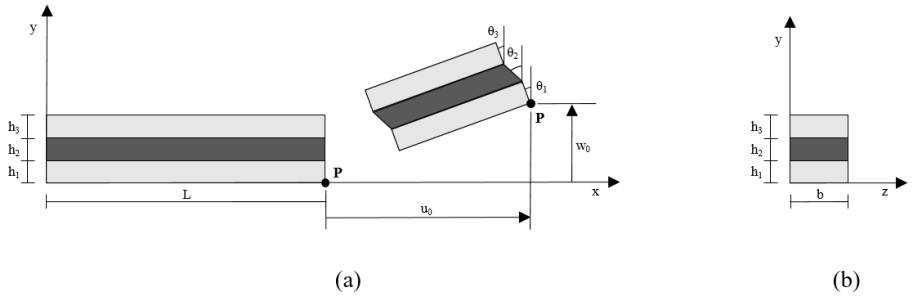


(a) (b)

Figure 2. Geometry and deformation kinematics for three-layers' beam element. (a) lateral view; (b) cross-section.

- It is not allowed slippage or delamination between layers, which means that continuity of displacement across the interfaces must be ensured.

- Transversal normal strains are neglected in all layers i.e., the transverse displacement is constant along the entire height of the multi-layer beam cross-section.
- The cross-sections of the layers remain plane after deformation and their rotation are treated independently, indicated by $\theta_i(t), i = 1, 2, 3$ in Figure 2. This enables to account for cross-section warping of the multi-layer beam.
- Isotropic and linear elastic behavior is assumed for the material of each layer.
- The vertical displacement of all layers is considered the same and is represented by $w_0(x, t)$.

The longitudinal displacement of each layer can be calculated using Eq. (1), in which $u_0$ represents the displacement of the bottom boundary of the first layer, $y$ represents the position along the $y-$axis, $h_i$ is the thickness of each layer, $\theta_i$ is the cross-section rotation angle of each layer, around the $z-$axis, and $t$ is time. Eq. (1) can be rewritten using Eq. (2):

$$u_i(x, y, t) = u_0(x, t) - \sum_{j=1}^{i-1} h_j \theta_j(x, t) - \left( y - \sum_{j=1}^{i-1} h_j \right) \theta_i(x, t), \tag{1}$$

$$\bar{y} = \left( y - \sum_{j=1}^{i-1} h_j \right). \tag{2}$$

The longitudinal and shear strains can be calculated using, respectively, Eqs. (3) and (4):

$$\epsilon_{xx}^i = \frac{\partial u_i}{\partial x} = \frac{\partial u_0}{\partial x} - \sum_{j=1}^{i-1} h_j \frac{\partial \theta_j}{\partial x} - \bar{y} \frac{\partial \theta_j}{\partial x}, \tag{3}$$

$$\gamma_{xy}^i = \frac{\partial u_i}{\partial y} + \frac{\partial w_i}{\partial x} = \frac{\partial w_0}{\partial x} - \theta_i. \tag{4}$$

The potential energy of the system is calculated using Eq. (5), in which $E_i$ and $G_i$ are, respectively, the Young's modulus and the shear modulus of the material of each layer:

$$U_i = \frac{1}{2} \int_V \left[ E_i \left( \epsilon_{xx}^i \right)^2 + G_i \left( \gamma_{xy}^i \right)^2 \right] dV. \tag{5}$$

The second moment of inertia of a rectangular cross-section, in relation to its base, can be calculated using the parallel axis theorem, as demonstrated in Eq. (6):

$$I_i = \frac{1}{12} b_i h_i^3 + A_i \left( \frac{h_i}{2} \right)^2 = \frac{1}{3} b_i h_i^3, \tag{6}$$

where $b_i$ is the width of each layer and $A_i$ is the cross-section area of each layer.

The potential energy of each layer can be rewritten as presented in Eq. (7):

$$U_i = \frac{1}{2} \int_0^L \left\{ E_i A_i \left[ (u_0')^2 - 2u_0' \left( \sum_{j=1}^{i-1} h_j \theta_j' \right) + \left( \sum_{j=1}^{i-1} h_j \theta_j' \right)^2 \right] + \right.$$
$$\left. + E_i A_i h_i \left[ \left( \sum_{j=1}^{i-1} h_j \theta_j' \right) \theta_i' - u_0' \theta_i' \right] + E_i I_i \left( \theta_i' \right)^2 + \kappa_i G_i A_i \left[ (w_0')^2 - 2w_0' \theta_i + \theta_i^2 \right] \right\} dx, \tag{7}$$

where $L$ is the element length and $\kappa_i$ is the shear-area correction factor.

The kinetic energy of each layer is calculated using Eq. (8):

$$T_i = \frac{1}{2} \int_0^L \int_{-\frac{h_i}{2}}^{\frac{h_i}{2}} b_i \rho_i \left[ (\dot{u}_i^c)^2 + \bar{y}^2 \left( \dot{\theta}_i \right)^2 + (\dot{w}_0)^2 \right] d\bar{y} dx, \tag{8}$$

where $\rho_i$ is the specific mass of the material of each layer and $\dot{u}_i^c$ is the axial velocity of the longitudinal line that passes through the cross-section center along each layer and can be obtained using Eq. (9):

$$\dot{u}_i^c = \dot{u}_0 - \sum_{j=1}^{i-1} h_j \dot{\theta}_j - \frac{h_i}{2} \dot{\theta}_i. \tag{9}$$

Developing Eq. (8) considering the mass per unit length presented in Eq. (10) and the mass moment of inertia per unit length, in relation to the cross-section center of each layer, presented in Eq. (11), one has the kinetic energy of each layer rewritten in Eq. (12).

$$m_i = \rho_i b_i h_i, \tag{10}$$

$$I^c_{M_i} = m_i \frac{h_i^2}{12}, \tag{11}$$

$$T_i = \frac{1}{2}\int_0^L \left\{ m_i \left[ \dot{u}_0^2 + \left( \sum\nolimits_{j=1}^{i-1} h_j \dot{\theta}_j \right)^2 + \frac{h_i^2}{4}\dot{\theta}_i^2 - 2\dot{u}_0 \left( \sum\nolimits_{j=1}^{i-1} h_j \dot{\theta}_j + \frac{h_i}{2}\dot{\theta}_i \right) + \right.\right.$$
$$\left.\left. + 2 \left( \sum\nolimits_{j=1}^{i-1} h_j \dot{\theta}_j \right) \frac{h_i}{2}\dot{\theta}_i \right] + I^c_{M_i}\dot{\theta}_i^2 + m_i \dot{w}_0^2 \right\} dx. \tag{12}$$

The total kinetic and potential energies of the three-layer beam element can be obtained by summing the energy contribution of each layer, as shown in Eqs. (13) and (14):

$$T = \sum\nolimits_{i=1}^{3} T_i, \tag{13}$$

$$U = \sum\nolimits_{i=1}^{3} U_i. \tag{14}$$

To enable to do the connections between the spectral elements of Figure 1, the kinetic and potential energies were written in terms of $u_i$, by applying Eqs. (15) – (19) into Eqs.(13) and (14):

$$\theta_1 = \frac{1}{h_1}\left(u_0 - u_1\right), \tag{15}$$

$$\theta_2 = \frac{1}{h_2}\left(u_1 - u_2\right), \tag{16}$$

$$\theta_3 = \frac{1}{h_3}\left(u_2 - u_3\right), \tag{17}$$

$$\theta_4 = \frac{1}{h_4}\left(u_3 - u_4\right), \tag{18}$$

$$\theta_5 = \frac{1}{h_5}\left(u_4 - u_5\right). \tag{19}$$

The system EOMs were obtained using Hamilton's Principle (Lanczos, 1986; Rade, 2018) and they are presented in Eqs. (20) – (24). The coefficients $p_s$ that appear in these equations are presented in Table 1.

$$p_0\ddot{u}_0 + p_1\ddot{u}_1 + p_2\ddot{u}_2 + p_3\ddot{u}_3 + p_4 u_0'' + p_5 u_1'' + p_6 u_2'' + p_7 u_3'' = 0, \tag{20}$$

$$p_8\ddot{w}_0 + p_9 w_0'' + p_{10}u_0' + p_{11}u_1' + p_{12}u_2' + p_{13}u_3' = 0, \tag{21}$$

$$p_{14}\ddot{u}_0 + p_{15}\ddot{u}_1 + p_{16}\ddot{u}_2 + p_{17}\ddot{u}_3 + p_{18}u_0'' + p_{19}u_1'' + p_{20}u_2'' + p_{21}u_3'' + p_{22}w_0' + p_{23}u_0 - p_{23}u_1 = 0, \tag{22}$$

$$p_{24}\ddot{u}_0 + p_{25}\ddot{u}_1 + p_{26}\ddot{u}_2 + p_{27}\ddot{u}_3 + p_{28}u_0'' + p_{29}u_1'' + p_{30}u_2'' + p_{31}u_3'' + p_{32}w_0' + p_{33}u_1 - p_{33}u_2 = 0, \tag{23}$$

$$p_{34}\ddot{u}_0 + p_{35}\ddot{u}_1 + p_{36}\ddot{u}_2 + p_{37}\ddot{u}_3 + p_{38}u_0'' + p_{39}u_1'' + p_{40}u_2'' + p_{41}u_3'' + p_{42}w_0' + p_{43}u_2 - p_{43}u_3 = 0. \tag{24}$$

The internal forces were obtained from boundary conditions related-terms, which appear naturally during application of Hamilton's Principle. These are presented in Eqs. (25) – (29).

$$Q_0 = p_4 u_0' + p_5 u_1' + p_6 u_2' + p_7 u_3', \tag{25}$$

$$V = p_9 w_0' + p_{10}u_0 + p_{11}u_1 + p_{12}u_2 + p_{13}u_3, \tag{26}$$

$$Q_1 = p_{18}u_0' + p_{19}u_1' + p_{20}u_2' + p_{21}u_3', \tag{27}$$

$$Q_2 = p_{28}u_0' + p_{29}u_1' + p_{30}u_2' + p_{31}u_3', \tag{28}$$

$$Q_3 = p_{38}u_0' + p_{39}u_1' + p_{40}u_2' + p_{41}u_3'. \tag{29}$$

Table 1. Coefficients $p_s$.

| | |
|---|---|
| $p_0 = -0.5\rho_1 A_1,$ | $p_{22} = \kappa_1 G_1 A_1,$ |
| $p_1 = -0.5\left(\rho_1 A_1 + \rho_2 A_2\right),$ | $p_{23} = -\frac{1}{h_1}\kappa_1 G_1 A_1,$ |
| $p_2 = -0.5\left(\rho_2 A_2 + \rho_3 A_3\right),$ | $p_{24} = 0,$ |
| $p_3 = -0.5\rho_3 A_3,$ | $p_{25} = 0.25h_2\rho_2 A_2 - \frac{1}{h_2} I^c_{m_2},$ |
| $p_4 = 0.5E_1 A_1,$ | $p_{26} = h_2\left(0.25\rho_2 A_2 + 0.5\rho_3 A_3\right) + \frac{1}{h_2} I^c_{m_2},$ |
| $p_5 = 0.5\left(E_1 A_1 + E_2 A_2\right),$ | $p_{27} = 0.5h_2\rho_3 A_3,$ |
| $p_6 = 0.5\left(E_2 A_2 + E_3 A_3\right),$ | $p_{28} = 0,$ |
| $p_7 = 0.5E_3 A_3,$ | $p_{29} = -0.5h_2 E_2 A_2 + \frac{1}{h_2} E_2 I_2,$ |
| $p_8 = -\left(\rho_1 A_1 + \rho_2 A_2 + \rho_3 A_3\right),$ | $p_{30} = -0.5h_2 E_3 A_3 - \frac{1}{h_2} E_2 I_2,$ |
| $p_9 = \kappa_1 G_1 A_1 + \kappa_2 G_2 A_2 + \kappa_3 G_3 A_3,$ | $p_{31} = -0.5h_2 E_3 A_3,$ |
| $p_{10} = -\frac{1}{h_1}\kappa_1 G_1 A_1,$ | $p_{32} = \kappa_2 G_2 A_2,$ |
| $p_{11} = \frac{1}{h_1}\kappa_1 G_1 A_1 - \frac{1}{h_2}\kappa_2 G_2 A_2,$ | $p_{33} = -\frac{1}{h_2}\kappa_2 G_2 A_2,$ |
| $p_{12} = \frac{1}{h_2}\kappa_2 G_2 A_2 - \frac{1}{h_3}\kappa_3 G_3 A_3,$ | $p_{34} = 0,$ |
| $p_{13} = \frac{1}{h_3}\kappa_3 G_3 A_3,$ | $p_{35} = 0,$ |
| $p_{14} = 0.25h_1\rho_1 A_1 - \frac{1}{h_1} I^c_{m_1},$ | $p_{36} = 0.25h_3\rho_3 A_3 - \frac{1}{h_3} I^c_{m_3},$ |
| $p_{15} = h_1\left(0.25\rho_1 A_1 + 0.5\rho_2 A_2\right) + \frac{1}{h_1} I^c_{m_1},$ | $p_{37} = 0.25h_3\rho_3 A_3 + \frac{1}{h_3} I^c_{m_3},$ |
| $p_{16} = 0.5h_1\left(\rho_2 A_2 + \rho_3 A_3\right),$ | $p_{38} = 0,$ |
| $p_{17} = 0.5h_1\rho_3 A_3,$ | $p_{39} = 0,$ |
| $p_{18} = -0.5h_1 E_1 A_1 + \frac{1}{h_1} E_1 I_1,$ | $p_{40} = -0.5h_3 E_3 A_3 + \frac{1}{h_3} E_3 I_3,$ |
| $p_{19} = -0.5h_1 E_2 A_2 - \frac{1}{h_1} E_1 I_1,$ | $p_{41} = -\frac{1}{h_3} E_3 I_3,$ |
| $p_{20} = -0.5h_1\left(E_2 A_2 + E_3 A_3\right),$ | $p_{42} = \kappa_3 G_3 A_3,$ |
| $p_{21} = -0.5h_1 E_3 A_3,$ | $p_{43} = -\frac{1}{h_3}\kappa_3 G_3 A_3.$ |

Writing the system in the frequency domain and assuming a transcendental function as solution along x-coordinate, one has:

$$u_0(x,t) = \frac{1}{N}\sum_{n=0}^{N-1}\tilde{U}_0(x,\omega)e^{i\omega_n t} = \frac{1}{N}\sum_{n=0}^{N-1}\left(\sum_{j=1}^{10} C_j e^{-ik_j x}\right)e^{i\omega_n t} = \frac{1}{N}\sum_{n=0}^{N-1}\mathbf{e}(x,\omega)\mathbf{c}e^{i\omega_n t}, \tag{30}$$

$$w_0(x,t) = \frac{1}{N}\sum_{n=0}^{N-1}W_0(x,\omega)e^{i\omega_n t} = \frac{1}{N}\sum_{n=0}^{N-1}\left(\sum_{j=1}^{10} \beta_{0,j} C_j e^{-ik_j x}\right)e^{i\omega_n t} = \frac{1}{N}\sum_{n=0}^{N-1}\mathbf{e}(x,\omega)\mathbf{B}_0\mathbf{c}e^{i\omega_n t}, \tag{31}$$

$$u_1(x,t) = \frac{1}{N}\sum_{n=0}^{N-1}\tilde{U}_1(x,\omega)e^{i\omega_n t} = \frac{1}{N}\sum_{n=0}^{N-1}\left(\sum_{j=1}^{10} \beta_{1,j} C_j e^{-ik_j x}\right)e^{i\omega_n t} = \frac{1}{N}\sum_{n=0}^{N-1}\mathbf{e}(x,\omega)\mathbf{B}_1\mathbf{c}e^{i\omega_n t}, \tag{32}$$

$$u_2(x,t) = \frac{1}{N}\sum_{n=0}^{N-1}\tilde{U}_2(x,\omega)e^{i\omega_n t} = \frac{1}{N}\sum_{n=0}^{N-1}\left(\sum_{j=1}^{10} \beta_{2,j} C_j e^{-ik_j x}\right)e^{i\omega_n t} = \frac{1}{N}\sum_{n=0}^{N-1}\mathbf{e}(x,\omega)\mathbf{B}_2\mathbf{c}e^{i\omega_n t}, \tag{33}$$

$$u_3(x,t) = \frac{1}{N}\sum_{n=0}^{N-1}\tilde{U}_3(x,\omega)e^{i\omega_n t} = \frac{1}{N}\sum_{n=0}^{N-1}\left(\sum_{j=1}^{10} \beta_{3,j} C_j e^{-ik_j x}\right)e^{i\omega_n t} = \frac{1}{N}\sum_{n=0}^{N-1}\mathbf{e}(x,\omega)\mathbf{B}_3\mathbf{c}e^{i\omega_n t}, \tag{34}$$

where:

$$\mathbf{e}(x,\omega) = \begin{bmatrix} e^{-ik_1 x} & e^{-ik_2 x} & e^{-ik_3 x} & e^{-ik_4 x} & e^{-ik_5 x} & e^{-ik_6 x} & e^{-ik_7 x} & e^{-ik_8 x} & e^{-ik_9 x} & e^{-ik_{10} x} \end{bmatrix}, \tag{35}$$

$$\mathbf{c} = \begin{bmatrix} C_1 & C_2 & C_3 & C_4 & C_5 & C_6 & C_7 & C_8 & C_9 & C_{10} \end{bmatrix}^T, \tag{36}$$

$$\mathbf{B}_m(\omega) = \mathrm{diag}[\beta_{m,j}], \qquad \text{for } m = 0,1,2,3, \tag{37}$$

and the variables $k_j$ are the wavenumbers, $C_j$ are arbitrary constants and $\beta_{m,j}$ are the components of wavemodes vector.

Equation (38) presents the eigenproblem through which the dispersion relation is obtained. The coefficients of Eq. (38) are presented in Table 2. The dispersion relation was solved for the wavenumbers using the MATLAB function *roots*, which has the Companion Matrix method implemented to find the roots of high order polynomials. The wavemodes were

obtained using the encountered wavenumbers.

$$\begin{bmatrix} X_{11} & X_{12} & X_{13} & X_{14} & X_{15} \\ X_{21} & X_{22} & X_{23} & X_{24} & X_{25} \\ X_{31} & X_{32} & X_{33} & X_{34} & X_{35} \\ X_{41} & X_{42} & X_{43} & X_{44} & X_{45} \\ X_{51} & X_{52} & X_{53} & X_{54} & X_{55} \end{bmatrix} \begin{Bmatrix} 1 \\ \beta_{0,j} \\ \beta_{1,j} \\ \beta_{2,j} \\ \beta_{3,j} \end{Bmatrix} = \begin{Bmatrix} 0 \\ 0 \\ 0 \\ 0 \\ 0 \end{Bmatrix}. \tag{38}$$

Table 2. Coefficients of Eq. (38).

| | | |
|---|---|---|
| $X_{11} = -p_0\omega^2 - p_4k^2,$ | $X_{25} = -p_{13}ik,$ | $X_{43} = -p_{25}\omega^2 - p_{29}k^2 + p_{33},$ |
| $X_{12} = 0,$ | $X_{31} = -p_{14}\omega^2 - p_{18}k^2 + p_{23},$ | $X_{44} = -p_{26}\omega^2 - p_{30}k^2 - p_{33},$ |
| $X_{13} = -p_1\omega^2 - p_5k^2,$ | $X_{32} = -p_{22}ik,$ | $X_{45} = -p_{27}\omega^2 - p_{31}k^2,$ |
| $X_{14} = -p_2\omega^2 - p_6k^2,$ | $X_{33} = -p_{15}\omega^2 - p_{19}k^2 - p_{23},$ | $X_{51} = -p_{34}\omega^2 - p_{38}k^2,$ |
| $X_{15} = -p_3\omega^2 - p_7k^2,$ | $X_{34} = -p_{16}\omega^2 - p_{20}k^2,$ | $X_{52} = -p_{42}ik,$ |
| $X_{21} = -p_{10}ik,$ | $X_{35} = -p_{17}\omega^2 - p_{21}k^2,$ | $X_{53} = -p_{35}\omega^2 - p_{39}k^2,$ |
| $X_{22} = -p_8\omega^2 - p_9k^2,$ | $X_{41} = -p_{24}\omega^2 - p_{28}k^2,$ | $X_{54} = -p_{36}\omega^2 - p_{40}k^2 + p_{43},$ |
| $X_{23} = -p_{11}ik,$ | $X_{42} = -p_{32}ik,$ | $X_{55} = -p_{37}\omega^2 - p_{41}k^2 - p_{43}.$ |
| $X_{24} = -p_{12}ik,$ | | |

To simplify the writing and understanding, the subscript "$_n$" was suppressed from $\omega_n$.

Equation (39) presents the vector of spectral nodal degrees of freedom (DOFs):

$$\mathbf{d} = \begin{Bmatrix} \tilde{U}_0(0) & W_0(0) & \tilde{U}_1(0) & \tilde{U}_2(0) & \tilde{U}_3(0) & \tilde{U}_0(L) & W_0(L) & \tilde{U}_1(L) & \tilde{U}_2(L) & \tilde{U}_3(L) \end{Bmatrix}^T. \tag{39}$$

Applying Eqs. (30) – (34) to the DOF vector (Eq. (39)), the relation of Eq. (40) is obtained:

$$\mathbf{d} = \mathbf{H}(\omega)\mathbf{c}, \tag{40}$$

where:

$$\mathbf{H}(\omega) = \begin{bmatrix} 1 & 1 & 1 & 1 & 1 & 1 & 1 & 1 & 1 & 1 \\ \beta_{0,1} & \beta_{0,2} & \beta_{0,3} & \beta_{0,4} & \beta_{0,5} & \beta_{0,6} & \beta_{0,7} & \beta_{0,8} & \beta_{0,9} & \beta_{0,10} \\ \beta_{1,1} & \beta_{1,2} & \beta_{1,3} & \beta_{1,4} & \beta_{1,5} & \beta_{1,6} & \beta_{1,7} & \beta_{1,8} & \beta_{1,9} & \beta_{1,10} \\ \beta_{2,1} & \beta_{2,2} & \beta_{2,3} & \beta_{2,4} & \beta_{2,5} & \beta_{2,6} & \beta_{2,7} & \beta_{2,8} & \beta_{2,9} & \beta_{2,10} \\ \beta_{3,1} & \beta_{3,2} & \beta_{3,3} & \beta_{3,4} & \beta_{3,5} & \beta_{3,6} & \beta_{3,7} & \beta_{3,8} & \beta_{3,9} & \beta_{3,10} \\ e_1 & e_2 & e_3 & e_4 & e_5 & e_6 & e_7 & e_8 & e_9 & e_{10} \\ \beta_{0,1}e_1 & \beta_{0,2}e_2 & \beta_{0,3}e_3 & \beta_{0,4}e_4 & \beta_{0,5}e_5 & \beta_{0,6}e_6 & \beta_{0,7}e_7 & \beta_{0,8}e_8 & \beta_{0,9}e_9 & \beta_{0,10}e_{10} \\ \beta_{1,1}e_1 & \beta_{1,2}e_2 & \beta_{1,3}e_3 & \beta_{1,4}e_4 & \beta_{1,5}e_5 & \beta_{1,6}e_6 & \beta_{1,7}e_7 & \beta_{1,8}e_8 & \beta_{1,9}e_9 & \beta_{1,10}e_{10} \\ \beta_{2,1}e_1 & \beta_{2,2}e_2 & \beta_{2,3}e_3 & \beta_{2,4}e_4 & \beta_{2,5}e_5 & \beta_{2,6}e_6 & \beta_{2,7}e_7 & \beta_{2,8}e_8 & \beta_{2,9}e_9 & \beta_{2,10}e_{10} \\ \beta_{3,1}e_1 & \beta_{3,2}e_2 & \beta_{3,3}e_3 & \beta_{3,4}e_4 & \beta_{3,5}e_5 & \beta_{3,6}e_6 & \beta_{3,7}e_7 & \beta_{3,8}e_8 & \beta_{3,9}e_9 & \beta_{3,10}e_{10} \end{bmatrix}, \tag{41}$$

and $e_j$ are the components of vector $\mathbf{e}(x,\omega)$, considering $x = L$.

From Eq. (40) and Eqs. (30) – (34), one has:

$$\tilde{U}_0(x,\omega) = \mathbf{e}(x,\omega)\mathbf{H}^{-1}(\omega)\mathbf{d}, \tag{42}$$

$$W_0(x,\omega) = \mathbf{e}(x,\omega)\mathbf{B}_0(\omega)\mathbf{H}^{-1}(\omega)\mathbf{d}, \tag{43}$$

$$\tilde{U}_1(x,\omega) = \mathbf{e}(x,\omega)\mathbf{B}_1(\omega)\mathbf{H}^{-1}(\omega)\mathbf{d}, \tag{44}$$

$$\tilde{U}_2(x,\omega) = \mathbf{e}(x,\omega)\mathbf{B}_2(\omega)\mathbf{H}^{-1}(\omega)\mathbf{d}, \tag{45}$$

$$\tilde{U}_3(x,\omega) = \mathbf{e}(x,\omega)\mathbf{B}_3(\omega)\mathbf{H}^{-1}(\omega)\mathbf{d}. \tag{46}$$

Applying Eqs. (42) – (46) into Eqs. (25) – (29) and using the signal convention of Figure 3, one has the SFEM model of the three-layers beam, shown in Eq. (47):

$$\mathbf{f} = \mathbf{S}(\omega)\mathbf{d}, \tag{47}$$

where $\mathbf{f}$ is the spectral nodal force vector (Eq. (48)) and $\mathbf{S}(\omega)$ is the spectral dynamic stiffness matrix.

$$\mathbf{f} = \begin{Bmatrix} Q_0(0) & V(0) & Q_1(0) & Q_2(0) & Q_3(0) & Q_0(L) & V(L) & Q_1(L) & Q_2(L) & Q_3(L) \end{Bmatrix}^T \tag{48}$$

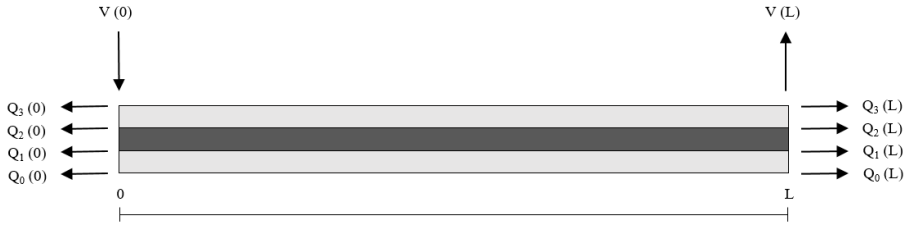


Figure 3. Signal convention used for three-layers spectral element.

To obtain the SFEM model of the one-layer beam, it is necessary just follow the same methodology, but adapting kinetic and potential energies for one layer, which means considering only three degrees of freedom per node ($u_0$, $w_0$ and $u_1$). The reinforced beam model (Figure 1) is assembled by coupling SFEM models of one and three-layers beam elements, by superposing their spectral dynamic stiffness matrices in the shared nodes, on the same manner that FEM models coupling is done.

## 3. MODEL VALIDATION

In order to guarantee the validity of the SFEM model proposed, the SFEM model of a three-layer beam element in free-free condition was compared with a FEM model built in the Simcenter FEMAP software. In Table 3, the parameters' values used to perform simulations are listed. The FEM model was built considering 100 beam elements, for which a single layer beam was used, with its thickness equal to the sum of the three layers thicknesses. It was not considered structural damping in these simulations. FEM results were obtained by doing a modal analysis, using the *solver* Simcenter Nastran. SFEM results were obtained by doing a harmonic analysis, with the left-hand first longitudinal DOF ($\tilde{U}_{0_1}$) being excited by a force with amplitude equal to $1$ N, and the displacement of the right-hand first longitudinal DOF ($\tilde{U}_{0_2}$) being measured. The natural frequencies were obtained by identifying which were the frequencies referring to the Frequency Response Function (FRF) curve peaks.

It was chosen to excite the longitudinal DOF to get the longitudinal and transversal modes of vibration. As can be seen in Eq. (1), if the excitation was transversal instead, the longitudinal modes of vibration would not be excited, because there are no coupling between $w_0$ and $u_0$. The displacement of longitudinal DOF was chosen to be evaluated, because it contains both transversal and longitudinal modes of vibration.

Table 3. Parameters used in the simulations for model validation.

| **Parameter** | **FEM (equivalent 1-layer)** | **SFEM (layer 1)** | **(layer 2)** | **(layer 3)** | **Unit** |
|---|---|---|---|---|---|
| $b$ | $0.05$ | $0.05$ | $0.05$ | $0.05$ | $\mathrm{m}$ |
| $h$ | $0.012$ | $0.004$ | $0.004$ | $0.004$ | $\mathrm{m}$ |
| $E$ | $70 \times 10^9$ | $70 \times 10^9$ | $70 \times 10^9$ | $70 \times 10^9$ | $\mathrm{Pa}$ |
| $\nu^*$ | $0.33$ | $0.33$ | $0.33$ | $0.33$ | - |
| $\kappa$ | $0.85$ | $0.85$ | $0.85$ | $0.85$ | - |
| $\rho$ | $2700$ | $2700$ | $2700$ | $2700$ | $\mathrm{kg/m^3}$ |

* $\nu$ is the Poisson's ratio.

In Table 4, the natural frequencies of the three-layer beam obtained from SFEM and FEM models are presented. The differences between the two models are small, being possible to assert that SFEM multi-layer beam model is accurate in representing the three-layer beam dynamic behavior. However, it is important to observe that the differences between SFEM and FEM results increased with frequency. One possible reason for that is the fact that it is necessary more refined meshes to represent high frequency phenomena using FEM. It is not the case of SFEM, because it is built using a transcendental interpolation function. It is important to highlight that in Table 4, the seventh mode is a longitudinal mode of vibration and the other ones are transversal modes of vibration.

## 4. DYNAMIC BEHAVIOR OF A BEAM WITH REINFORCEMENTS

In the previous sections, a methodology to calculate the dynamic stiffness matrix of a multi-layer beam was presented and validated. In this section, the influence of the weakness, introduced by a gap in the primary beam, and of the length of the reinforcement on the dynamic behavior of a beam is investigated.

Consider the beam shown in Figure 1, consisting of layers with a rectangular cross-sectional area and the same material

Table 4. Comparison of the natural frequencies of a three-layer beam element with $L = 0.5\ \mathrm{m}$, obtained using the SFEM, with those of an equivalent 1-layer beam obtained using the FEM (FEMAP).

| **Mode number** | 1 | 2 | 3 | 4 | 5 | 6 | 7 | 8 |
|---|---|---|---|---|---|---|---|---|
| **SFEM (Hz)** | 250.7 | 688.1 | 1340.8 | 2198.9 | 3252.8 | 4491.7 | 5091.8 | 5903.6 |
| **FEMAP (Hz)** | 250.6 | 688.0 | 1340.8 | 2199.5 | 3255.0 | 4496.9 | 5091.5 | 5913.5 |
| *% difference with FEMAP* | 0.0399 | 0.0145 | 0.0000 | 0.0273 | 0.0676 | 0.1156 | 0.0059 | 0.1674 |

properties. The total length of the primary beam layer ($L_{beam}$), which appears in subsections A and B, is assumed to be constant and has a value of $0.2\ \mathrm{m}$. To evaluate the influence of the reinforcement layer length ($L_R$), four lengths are considered in this analysis: $25\%$, $50\%$, $75\%$ and $100\%$ of the primary beam length. For each reinforcement case, four gap lengths are evaluated, which comprehend values of $0\%$, $25\%$, $50\%$ and $75\%$ of the reinforcement length. The lengths of subsections are summarized in Table 5. The material properties and the width, thickness and shear-area correction factor are those presented in SFEM columns of Table 3.

Table 5. Elements lengths ($L$) for different system configurations. Reported values are in meters.

| | $\mathbf{0.25\ L_{beam}}$ | | $\mathbf{0.50\ L_{beam}}$ | | $\mathbf{0.75\ L_{beam}}$ | | $\mathbf{1.00\ L_{beam}}$ | |
|---|---|---|---|---|---|---|---|---|
| **"C1"** | **"A"** | **"B"** | **"A"** | **"B"** | **"A"** | **"B"** | **"A"** | **"B"** |
| **0** | 0.17500 | 0.02500 | 0.15000 | 0.05000 | 0.12500 | 0.07500 | 0.10000 | 0.10000 |
| $\mathbf{0.25\ L_R}$ | 0.18125 | 0.01875 | 0.16250 | 0.03750 | 0.14375 | 0.05625 | 0.12500 | 0.07500 |
| $\mathbf{0.50\ L_R}$ | 0.18750 | 0.01250 | 0.17500 | 0.02500 | 0.16250 | 0.03750 | 0.15000 | 0.05000 |
| $\mathbf{0.75\ L_R}$ | 0.19375 | 0.00625 | 0.18750 | 0.01250 | 0.18125 | 0.01875 | 0.17500 | 0.02500 |

Using the SFEM multi-layer beam model derived in Section 2, the dynamic stiffness for each of the subsections depicted as A, B and C in Figure 1 is obtained. Then, following a similar procedure to the finite element methods, the dynamic stiffness matrix of each beam subsection is concatenated to form the dynamic stiffness matrix of the entire structure. Harmonic analyses are done to obtain the natural frequencies of the structure for all studied cases. It was chosen to be analyzed only the transversal vibrations of the reinforced beam. Thus, a transversal force with $1\ \mathrm{N}$ of amplitude is applied at the left-hand end of the structure and the receptance of the transverse displacement at the right-hand end of the structure is calculated, considering each of the reinforcement and gap lengths. The results are plotted in Figure 4 for a frequency range from $0$ up to $2000$ Hz. In particular, Figure 4(a-d) show, respectively, the cases of beams with reinforcement lengths values of $25\%$, $50\%$, $75\%$, and $100\%$ of the primary beam length. To avoid large-amplitude resonant peaks, a structural damping of $1\%$ was considered.

To support the analysis of the influence of the reinforcement and gap lengths on the dynamic behavior of the structure, the first four natural frequencies for each of the cases are summarized in Table 6. The reinforcements lengths investigated are represented in Figure 4 and in Table 6 with the letter "$R$" followed by the respective percentage, while the gap lengths studied are represented by letter "$G$" followed by the respective percentage.

Table 6. Comparison of the natural frequencies of the reinforced beam for different gap and reinforcement lengths, obtained using SFEM. Reported values are in Hz.

| | | **R025** | | | | | **R050** | | |
|---|---|---|---|---|---|---|---|---|---|
| **Mode** | **G000** | **G025** | **G050** | **G075** | **Mode** | **G000** | **G025** | **G050** | **G075** |
| 1 | 139.5 | 132.2 | 125.5 | 119.6 | 1 | 169.2 | 148.3 | 131.4 | 117.5 |
| 2 | 357.4 | 387.0 | 425.7 | 450.1 | 2 | 355.6 | 347.9 | 353.7 | 360.2 |
| 3 | 750.6 | 709.4 | 672.3 | 638.3 | 3 | 928.7 | 815.3 | 720.8 | 640.1 |
| 4 | 1144.5 | 1401.5 | 1452.3 | 1390.5 | 4 | 1212.4 | 1189.4 | 1086.1 | 896.5 |
| | | **R075** | | | | | **R100** | | |
| **Mode** | **G000** | **G025** | **G050** | **G075** | **Mode** | **G000** | **G025** | **G050** | **G075** |
| 1 | 221.7 | 175.8 | 143.2 | 119.2 | 1 | 308.6 | 217.0 | 160.0 | 122.9 |
| 2 | 380.7 | 326.8 | 286.9 | 253.6 | 2 | 464.2 | 337.3 | 255.2 | 200.6 |
| 3 | 1163.0 | 967.3 | 796.1 | 657.8 | 3 | 1207.6 | 1119.5 | 885.5 | 674.3 |
| 4 | 1489.1 | 1182.5 | 896.9 | 719.0 | 4 | 1999.2 | 1316.9 | 906.0 | 702.8 |

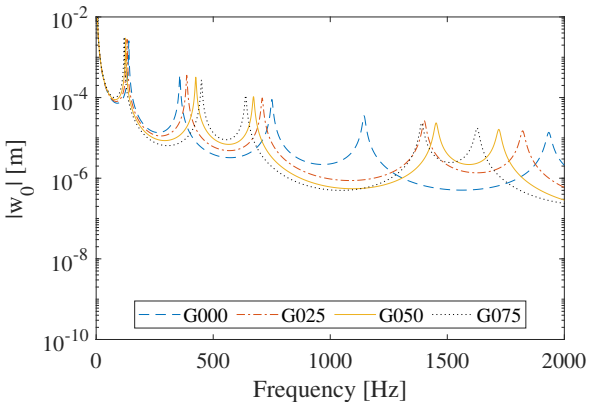


(a) R025 for varying gap size.

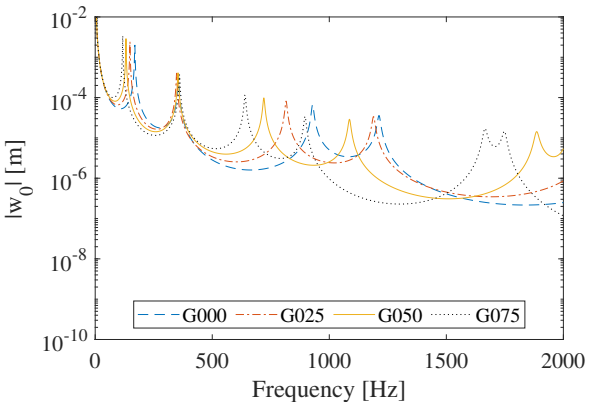


(b) R050 for varying gap size.

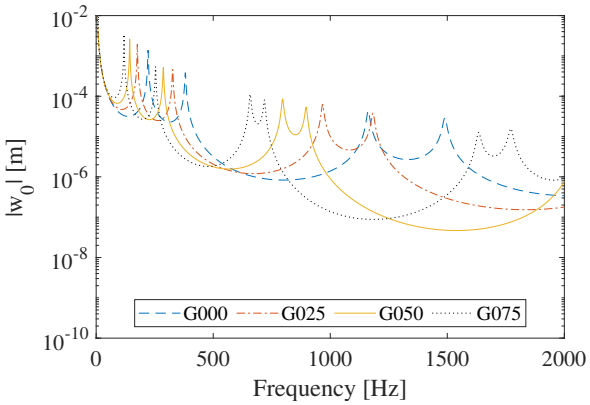


(c) R075 for varying gap size.

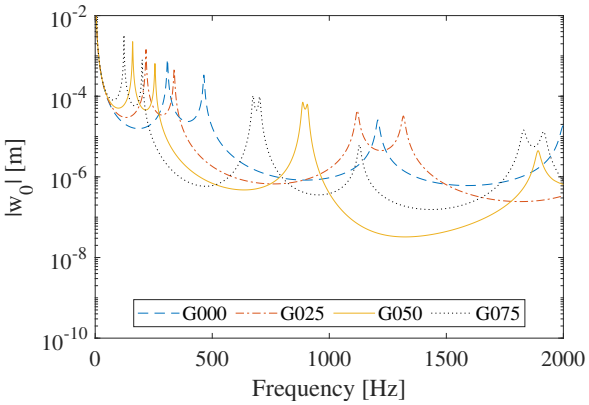


(d) R100 for varying gap size.

Figure 4. FRF plots of the transverse displacement of the right-hand end of the structure shown in Figure 1, for different reinforcement and gap lengths, obtained using the SFEM. The reinforcement corresponding to (a) 25%; (b) 50%; (c) 75%; and (d) 100% of the primary beam length are presented.

Examining Figure 4, it can be seen that for all reinforcement lengths almost all natural frequencies of the structure decreased with the increase of the gap length, which means that in general increasing the gap length softens the structure. This can also be observed by analyzing Table 6. Additionally, it is noted that for a structure without gap, increasing the length of the reinforcement layer improves the structural properties, making the beam stiffer, with exception of the second mode of vibration for reinforcements sizes R025 and R050. The same tendency can be seen for gap value of 25% of the reinforcement length, but it is not true for all modes of vibration, because for some of them the natural frequencies are greater for smaller reinforcements, as shown in Table 6. For gap values corresponding to 50% and 75%, with some exceptions, increasing the reinforcement length made the beam stiffer in the first and third modes of vibration, shifting the respective natural frequencies to higher frequencies, but it showed a detrimental effect in the second and fourth modes of vibration, shifting the natural frequencies of these modes of vibration to lower frequencies. Thus, it is clear that to improve the dynamic properties of the system, the length of reinforcement layers that are effectively bonding the primary beam is important.

## 5. CONCLUSIONS

This paper investigates the influence of reinforcement layers to improve the dynamic behavior of a beam with a weakness point. The weakness in the structure is introduced by creating a gap between the left- and right-hand primary beams. The influence of the gap length was also investigated. The system dynamics were analyzed using the dynamic stiffness matrix calculated from the Spectral Finite Element Method (SFEM) derived for a multi-layer beam. Four reinforcement lengths were considered in the analysis, and for each of these cases four gap lengths were also considered. It was demonstrated that increasing the gap length creates detrimental effects in some modes of vibration, by reducing the stiffness of the structure in these modes and consequently shifting the respective natural frequencies to lower values. This phenomenon becomes more significant at higher frequencies where the effects of the shear modulus are dominant. For the case without gap, increasing the reinforcement presented an improvement in the dynamics of the structure, making it stiffer. When the gap represented 25% of the reinforcement length, the same tendency was observed, but not for all modes

of vibration. For the cases where the gap represented $50\%$ and $75\%$, the increase of the reinforcement layers improved the structural properties of the beam in the first and third modes of vibration, but had a detrimental effect in these properties in the second and fourth modes of vibration.

## 6. ACKNOWLEDGEMENTS

The authors would like to acknowledge the financial support of the São Paulo Research Foundation (FAPESP), Grant numbers 2018/15894-0, 2021/11258-5, 2022/11995-2 and 2022/09543-6 and CNPq – National Council for Scientific and Technological Development, 312068/2020-4, 162679/2021-1 and 407545/2022-0. Authors also thank funding by the company PLP Brazil, established through a technical-scientific cooperation agreement.

## 7. REFERENCES

Azandariani, M.G., Gholami, M. and Zare, E., 2022. "Development of spectral element method for free vibration of axially-loaded functionally-graded beams using the first-order shear deformation theory". *European Journal of Mechanics - A/Solids*, Vol. 96, p. 104759.

Banerjee, J.R., Cheung, C.W., Morishima, R., Perera, M. and Njuguna, J., 2007. "Free vibration of a three-layered sandwich beam using the dynamic stiffness method and experiment". *International Journal of Solids and Structures*, Vol. 44, pp. 7543–7563.

Banerjee, J. and Sobey, A., 2005. "Dynamic stiffness formulation and free vibration analysis of a three-layered sandwich beam". *International Journal of Solids and Structures*, Vol. 42, pp. 2181–2197.

Doyle, J.F., 2012. *Wave Propagation in Structures: Spectral Analysis Using Fast Discrete Fourier Transforms*. Mechanical Engineering Series. Springer New York.

Hart-Smith, L.J., 1973a. "Adhesive-bonded double-lap joints". National Aeronautics and Space Administration, Langley Research Center.

Hart-Smith, L.J., 1973b. "Non-classical adhesive-bonded joints in practical aerospace construction". National Aeronautics and Space Administration, Langley Research Center.

Hollaway, L. and Cadei, J., 2002. "Progress in the technique of upgrading metallic structures with advanced polymer composites". *Progress in Structural Engineering and Materials*, Vol. 4, pp. 131–148.

Lanczos, C., 1986. *The Variational Principles of Mechanics*. Dover Publications, New York.

Lee, U., 2009. *Spectral Element Method in Structural Dynamics*. John Wiley and Sons (Asia) Pte Ltd, Singapore.

Perrut, V.A., 2018. *Estudo do comportamento estático e à fadiga de junta colada compósito polimérico e aço em diferentes tratamentos de superfície e sujeita à névoa salina aplicada como reparo na indústria do petróleo*. Ph.D. thesis, Postgraduate Program in Metallurgical and Materials Engineering, COPPE, of Federal University of Rio de Janeiro, Rio de Janeiro, Brazil.

Rade, D.A., 2018. *Cinemática e Dinâmica para Engenharia*. Elsevier, Rio de Janeiro.

Smyczynski, M. and Magnucka-Blandzi, E., 2015. "Static and dynamic stability of an axially compressed five-layer sandwich beam". *Thin-Walled Structures*, Vol. 90, pp. 23–30.

Su, H. and Banerjee, J., 2015. "Development of dynamic stiffness method for free vibration of functionally graded timoshenko beams". *Computers and Structures*, Vol. 147, pp. 107–116.

Sun, R., Xie, B., Perera, R. and Pan, Y., 2018. "Modeling of reinforced concrete beams exposed to fire by using a spectral approach". *Advances in Materials Science and Engineering*, Vol. 2018, pp. 1–12.

Unal, A., Wang, G. and Zuo, Q.H., 2016. "Modeling and analysis of multilayered elastic beam using spectral finite element method". *Journal of Vibration and Acoustics*, Vol. 138, p. 041013.

Xu, R. and Wu, Y., 2007. "Two-dimensional analytical solutions of simply supported composite beams with interlayer slips". *International Journal of Solids and Structures*, Vol. 44, pp. 165–175.

Zhao, X.L. and Zhang, L., 2007. "State-of-the-art review on frp strengthened steel structures". *Engineering Structures*, Vol. 29, No. 8, pp. 1808–1823.

## 8. RESPONSIBILITY NOTICE

The authors are the only responsible for the printed material included in this paper.